

# **Tensile and thermal properties of low-melt poly aryl ether ketone reinforced with continuous carbon fiber manufactured by robotic 3D printing**

Seyed Miri<sup>1</sup>, Jordan Kalman<sup>1</sup>, Jean-Philippe Canart<sup>2</sup>, Joe Spangler<sup>2</sup>, Kazem Fayazbakhsh<sup>1\*</sup>

<sup>1</sup>Department of Aerospace Engineering, Toronto Metropolitan University, Toronto, Ontario M5B2K3, Canada

<sup>2</sup>Teijin Carbon America, Inc., 121 Cardiff Valley Rd, Rockwood, TN 37854, USA

\*Corresponding author: kazem@ryerson.ca; Tel: (+1) 416-979-5000 ext. 556414; fax: (+1) 416-979-5056; <https://orcid.org/0000-0003-3963-8282>

## **Abstract**

Fused Filament Fabrication (FFF) can 3D print final parts from continuous carbon fiber composites with high structural and thermal performance. This study uses a robotic 3D printer to manufacture tensile specimens from Low-Melt Poly Aryl Ether Ketone (LM PAEK) reinforced with continuous carbon fiber per ASTM D3039-17. A total of 18 tensile specimens are 3D printed to investigate the impact of the nozzle temperature, bed temperature, layer thickness, and the number of layers. Maximum tensile strength and modulus of 1282.1 MPa and 111.9 GPa, respectively, are achieved. These values are, respectively, 32.4% and 79.0% higher than the maximum reported results in the literature for thermoplastic composites made from FFF 3D printing. The build platform temperature of 165 °C results in a specimen without cold crystallization as 3D printed with 20.2% degree of crystallinity and a  $T_g$  of 154.79 °C. A uniform distribution of fibers and minimum voids and gaps are observed in the specimen cross-section.

**Keywords:** Fused Filament Fabrication (FFF); Robotic 3D printing; Low-Melt Poly Aryl Ether Ketone (LM PAEK); Continuous carbon fiber composites; Tensile properties; Degree of Crystallinity.

**International Journal of Advanced Manufacturing Technology**

<https://doi.org/10.1007/s00170-022-09983-7>

## 1. Introduction

Fused Filament Fabrication (FFF) technology has been improved and utilized extensively in the aerospace industry to rapidly manufacture prototypes, tooling, and small production parts currently used on the latest commercial aircraft. Continuous fiber reinforced thermoplastic composites have shown encouraging results in improving mechanical and physical properties of final 3D printed parts. Table 1 summarizes the studies reporting the experimental tensile properties of continuous fiber reinforced thermoplastic composites fabricated using FFF 3D printing [1-15].

**Table 1. Tensile properties of 3D printed parts from continuous fiber reinforced polymers.**

Ref	Fiber Material	Matrix Material	V <sub>f</sub> (%)	UTS (MPa)	Young's Modulus (GPa)	Printer Type	Process
[1]	Carbon	Nylon	34.5	475	35.7	Mark One®	(1)
[2]	Kevlar	Nylon	10.1	82	9.00	Mark One®	(1)
[3]	Kevlar	Nylon	16.7	150	8.50	Mark One®	(1)
	Carbon		14.1	255	21.7		
[4]	Carbon	Nylon	27.0	986	62.5	Mark One®	(1)
[5]	Carbon	Nylon	11.0	216	7.73	Mark One®	(1)
[6]	Carbon	Nylon	N/A	110	3.94	Mark Two®	(1)
[7]	Carbon	Nylon	20.0	104	44.3	Mark Two®	(1)
[8]	Carbon	Nylon	54.0	304	23.7	Mark Two®	(1)
[9]	Carbon	Nylon	47.0	719	40.0	Mark Two®	(1)
[10]	Carbon & Jute	PLA	6.60	185	19.5	FlashForge®	(2)
[11]	CNT	Ultem 1010	27.8	317*	19.5*	Aleph®	(2)
[12]	Carbon bundle 1k	PLA	9.62	111	12.2	COMBOT-I®	(2)
[13]	Carbon bundle 1k	ABS	N/A	147	4.20	Custom Built	(2)
[14]	Carbon bundle 1k	PLA	34.0	91.0	3.25	Custom Built	(2)
[15]	E-Glass	PLA	50.0	478	29.4	Custom Built	(2)

Process (1): Prepreg filaments

Process (2): Dry fiber mixed with a thermoplastic resin at the nozzle

\* - Specific values reported per  $g/cm^3$

Most researchers have used prepreg filaments reinforced with continuous fibers from Markforged to manufacture parts using their desktop 3D printers [1-8]. Van Der Klift et al. [1] 3D printed specimens with ten layers of 0.125 mm each by alternating layers with pure Nylon and carbon fiber prepreg filament. They reported tensile strength of 475 MPa and a modulus of 35.7 GPa. However, the testing procedures fail to follow any ASTM standards. In addition, the 3D printed specimens consist of repeating layers of carbon fiber reinforced polymer (CFRP) sandwiched within pure Nylon. The resulting fiber volume fraction is estimated using a theoretical formula and Markforged published data. Melenka et al. [2] manufactured Kevlar reinforced Nylon

specimens with varying fiber volume fractions of 4.04%, 8.08%, and 10.1%. The specimens were tested according to ASTM D638-14 with resulting elastic moduli of 1.77 GPa, 6.92 GPa, and 9.00 GPa, respectively. They studied the dimensional accuracy of the Mark One printer by comparing manufactured specimens to their nominal width and thickness dimensions of 19.0 mm and 3.20 mm, respectively. A maximum percentage difference in the specimen width and thickness were reported as 1.02% and 3.81% larger than the nominal values, respectively. Lastly, waviness in the Kevlar yarns was observed in the printed specimens and concluded to be caused by a lack of fiber tensioning during the printing process. Oztan et al. [3] studied the microstructure and mechanical properties of 3D printed continuous fiber composites using a Mark One printer. Both Kevlar and carbon fiber (CF) reinforced Nylon specimens were manufactured per ASTM D3039. The strength and stiffness of the Markforged material were reported as approximately 30-40% weaker than traditional composites. Blok et al. [4] compared the mechanical properties of chopped and continuous CF-reinforced Nylon using the ASTM D638 and D3039 coupons, respectively. They tested four specimens and reported a characteristically high tensile strength of 986 MPa and a modulus of 62.5 GPa. The authors stated that the experimental tensile strength exceeded the properties outlined by the material supplier by over 20%. Dickson et al. [5] investigated the mechanical properties of continuous glass, aramid, and CF-reinforced Nylon composites. It was found that the continuous CF-reinforced Nylon exhibited the highest mechanical properties of the three materials. Mei et al. [6] examined printing configurations based on concentric rings of fiber embedded into matrix core by altering fill patterns and fiber-matrix ratio. However, they did not report the fiber volume fraction of the final specimens. González-Estrada et al. [7] manufactured samples with a layer height of 0.1 mm, consisting of 26 layers of pure Nylon and six layers of carbon fiber reinforcement, totaling 32 layers. Naranjo-Lozada et al. [8] presented an evaluation of the impact of various geometric parameters on the resulting tensile properties of both chopped and continuous CF-reinforced Nylon. The highest volume fraction reported was 54%, with a maximum tensile strength and modulus of 304 MPa and 23.7 GPa, respectively. Pyl et al. [9] manufactured ASTM D638-14 and D3039 coupons to explore the potential of 3D printing freeform continuous CF-reinforced Nylon. The maximum tensile strength and modulus were 719 MPa and 58.1 GPa, respectively. Markforged composite filaments are currently limited to one polymer material, Nylon, and their desktop 3D printers have a small build volume of 32 cm × 13 cm × 15 cm for the Mark Two.

To remove Markforged materials and 3D printer limitations, including the slicer software, researchers used other commercially available FFF 3D printers to manufacture composite specimens for mechanical testing [10-12]. Matsuzaki et al. [10] 3D printed specimens using carbon and jute fiber reinforced PLA at the nozzle entrance and found ultimate tensile strength and tensile modulus of 185 MPa and 19.5 GPa, respectively. This corresponds to a respective improvement of 600% and 435% to pure PLA. They also reported uneven distribution of the fibers and observed localized entanglement. Lastly, they concluded the results should not be taken as reference values since test procedures were based on the Japanese Industrial Standards Committee, JIS K7162, and not ASTM standards. Gardner et al. [11] 3D printed samples by combining carbon nanotube (CNT)

yarns and Ultem 1010 (Polyetherimide) matrix having 27.8% fiber volume fraction and reported improved specific properties for single and dual nozzle printers. They tested the 3D printed specimens per ASTM D638 and reported a 287% increase in specific strength ( $317 \text{ MPa}/(\text{g}/\text{cm}^3)$ ) and 1850% improvement in specific modulus ( $19.5 \text{ GPa}/(\text{g}/\text{cm}^3)$ ) compared to that of pure Polyetherimide ( $82 \text{ MPa}/(\text{g}/\text{cm}^3)$  &  $1.0 \text{ GPa}/(\text{g}/\text{cm}^3)$ ), respectively. Yin et al. [12] fabricated CF-reinforced PLA composites with a volume fraction of CF to PLA matrix of 9.62%. The reported maximum tensile strength and modulus values were 111 MPa and 12.2 GPa, respectively.

Researchers also added custom-built components to commercially available FFF 3D printers to manufacture composite specimens for mechanical testing [13-15]. Yang et al. [13] used a double extruder printer to manufacture samples by combining a 1k strand bundle of carbon fiber yarn with pure ABS at the nozzle entrance. They achieved an ultimate tensile strength of 147 MPa, corresponding to a 294% improvement compared to pure ABS (50.0 MPa) and Young's modulus of 4.18 GPa, nearly twice that of pure ABS. Li et al. [14] experimented by modifying 1k strands of carbon fiber bundles through a magnetic stirring process to increase their interfacial bonding characteristics with PLA matrix. A methylene dichloride solution was used to partially dissolve PLA resin which was then incorporated with emulsifying and antifoaming agents. This solution was then used to modify the surface of the carbon fibers before printing the specimens. The manufactured specimens had an estimated volume fraction of 34%. They reported a 325% improvement in the ultimate tensile strength (from 28 to 91 MPa) and 266% improvement in Young's modulus (1.22 to 3.25 GPa). Akhoundi et al. [15] investigated the parameters which influence the mechanical properties of continuous glass fiber-reinforced PLA specimens using a FFF style 3D printer. A nozzle width of 0.3 mm, layer height of 0.22 mm, and a rectilinear infill pattern were used. The reported fiber volume fraction was 50% resulting in maximum tensile strength and modulus of 478 MPa and 29.4 GPa, respectively.

The previous studies used filaments with a circular cross-section processed through circular nozzles, inherently producing voids between extrudates and layers. In addition, the application of any compacting force causes fiber strands to distribute unevenly and, in some cases, twist or tangle together, creating manufacturing defects. The prepreg filaments only used low-temperature thermoplastics, e.g., Nylon, PLA, and ABS, limiting the application of the final parts in the industry. Continuous CF-reinforced Poly Aryl Ether Ketones (PAEKs) are among the highest performance thermoplastic composites currently in use and under qualification for aerospace structural applications [16]. One member of the PAEK family known as low-melt (LM) PAEK is a slow-crystallizing polymer compared to PEEK and requires lower melt temperature while maintaining exceptional properties. The melting temperature of LM PAEK is approximately  $40^\circ\text{C}$  lower than PEEK (i.e.,  $304^\circ\text{C}$  vs.  $346^\circ\text{C}$ ) [17]. LM PAEK is best suited for AM processes using filament, powder, and prepreg tape feedstocks. In addition to lower required processing temperatures, the out-of-plane or interlayer strength has been reported to exceed that of PEEK manufactured via material extrusion (MEX) 3D printing.

The previous studies [1-15] used desktop 3D printers for fabrication, e.g., Mark Two, which are three-axis gantry-based machines with limited build volume. Robotic 3D printers can increase the build volume and manufacturing flexibility compared to conventional desktop machines. They combine a 3D printing head to extrude materials with a multi-axis robotic arm. Researchers primarily have used robotic 3D printing in construction [18, 19] and architecture [20] using concrete and mineral foam, respectively. While several companies have developed their own robotic 3D printers for continuous fiber reinforced thermoplastics [21], research studies in this field, especially on high-temperature thermoplastics, are rare.

This work addresses the limitations of the previous research studies by: (1) processing a prepreg tape with a rectangular cross-section; (2) using a high-temperature thermoplastic, LM PAEK, reinforced with continuous carbon fiber as feedstock; and (3) developing a six-axis robotic 3D printing that can process continuous fiber-reinforced high-temperature thermoplastic composites, and can be easily scaled up for large format manufacturing.

In this paper, first, the robot cell, including an ABB IRB1200 robot, build platform, and a custom-built 3D printing head with a slotted nozzle is presented. Second, the programming process and software used for communication between the robot and the 3D printing head for manufacturing parts are described. Next, manufacturing process and design parameters are provided for the fabrication of tensile specimens. Their leftovers are used for the degree of crystallinity test and Scanning Electron Microscopy (SEM) of the cross-sections. Experimental results are presented in Section 3, and are compared with values obtained from the literature (Table 1). Finally, the paper wraps up with conclusions and recommendations for future research studies in the field.

## **2. Methodology**

### ***2.1. Robotic 3D printing***

A six-axis ABB IRB1200 robot was selected for its flexibility, large size (arm reach of 90 cm), and controllability through communication with a programmable logic controller (PLC) port. The payload carrying capacity of 5 kg and high holding force allow for heavy payloads and the possibility of compacting the deposited material. Developing the system on an ABB robot also allows for the rapid implementation of the technology to larger robots since the system is designed around the ABB RAPID code library industrial robot controller, IRC5. A 3D printing head is attached to the robot, and the robot is installed on a metallic table surrounded by a protective enclosure. The robot cell is designed to accommodate a  $304.8 \times 304.8$  mm (12 in.  $\times$  12 in.) heated bed to manufacture large continuous fiber composite parts (Figure 1). The heated bed is a stainless-steel plate fitted with heating elements under its surface and covered by a one-inch width self-adhesive Kapton tape on the top surface.

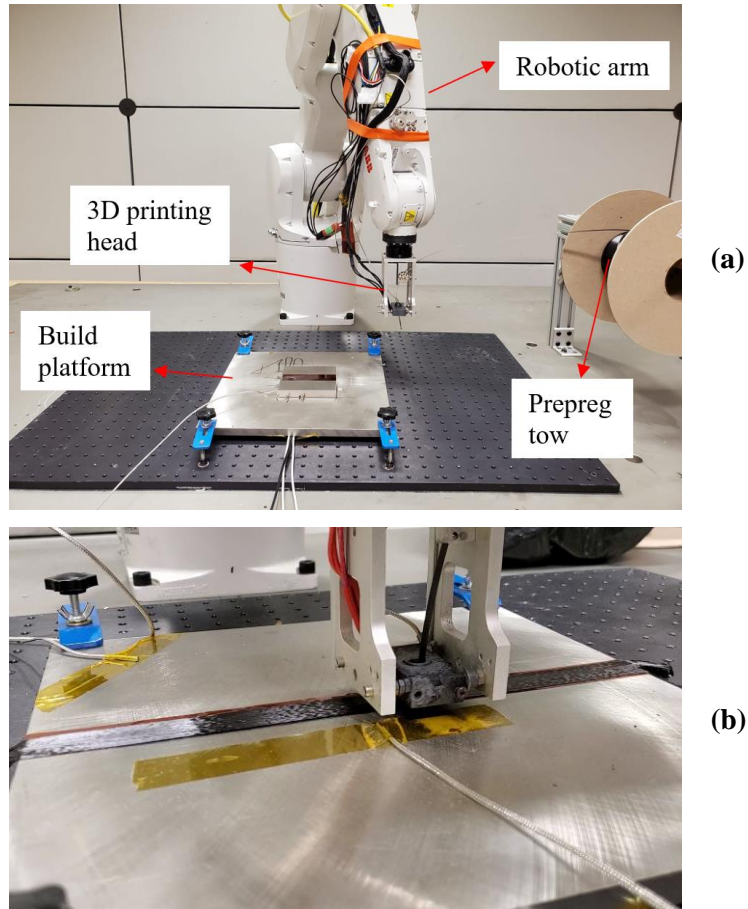


**Figure 1. The robotic 3D printer: (a) overview of the system; (b) close-up view of the 3D printing head and the build platform.**

A tape with a rectangular cross-section would lose its shape around a circular nozzle exit (a cylinder). It would result in entanglement and twist of the fiber bundles during 3D printing. As a result, a nozzle with a slot exit is designed and built to guide and deposit the prepreg tape with more accuracy and better fiber alignment. Figure 2 shows the selected design and the final manufactured nozzle. A mild-steel bushing holds two identical stainless steel dowel pins parallel, leaving a slot opening between them. Dowel pin's diameter is 3.0 mm, and the two pins are separated by 4.0 mm, leaving a 1.0 mm gap between them. Pins were hardened to 54-58 RC, appropriate for an abrasive material, like the carbon fiber prepreg tape. The sharp edges between the mild-steel bushing and dowel pins can cause carbon fibers to entangle, creating cotton balls inside the nozzle. In future studies, thick hard chrome plating will be used to fill any microscopic gaps and sharp edges in the nozzle.

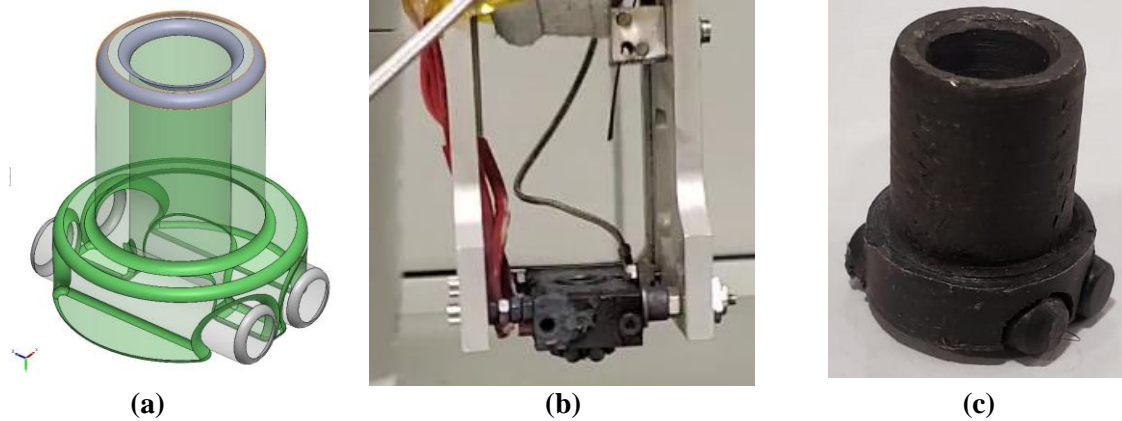


**Figure 2. The slotted nozzle: (a) the CAD model; and (b) the nozzle inside the heating block; and (c) the nozzle showing the dowel pins.**

The 3D printing head is designed and built to work in synchronicity with the ABB robot movements. The prepreg tape is initially fed into the nozzle through a guided slot, and is kept taut (under low tension loads) during the printing process. After the fiber passes through the nozzle, it is tacked and dragged onto the bed. The RAPID code is generated through RoboDK, an offline programming software package used to program industrial robots. A CAD model of the tool is designed in CATIA V5, which is imported into the software. The center of the nozzle tip is considered for the generation of the tool center point (TCP). The CAD model typically is close to the exact TCP of the final tool. Still, corrections need to be made to compensate for manufacturing tolerances and other physical discontinuities such as thermal expansion. Cura Lulzbot Edition 4.10, as an open-source slicing software, was used to create G-codes based on toolpath. The RoboDK toolpaths are then post-processed into RAPID code to be read by the robot. The code is uploaded to the IRC5 controller, and once the robot orientation is set to a favorable position to avoid unexpected motions, the program is started. Nozzle and build platform temperatures are monitored and controlled by the IRC5 through serial communications with a PLC box.

## ***2.2. Specimen design and manufacturing***

Tensile specimens per ASTM D3039-17 with fibers along their length ( $0^\circ$  fiber orientation) are 3D printed flat on the build platform, XYZ build orientation per ISO/ASTM 52921:2013(E) [22]. Since this study aims to find the maximum mechanical and thermal performance of final parts, 100% infill (no gaps) strategy is utilized, which uses the prepreg tow width after 3D printing in its programming. In a manufacturing trial, 3D printing speed of 5 mm/s was found to be optimum and is used here. It should be noted that 40 mm/s (2400 mm/min) is a typical speed used for FFF 3D printing of pure low-temperature polymers. The feedstock, Tenax<sup>TM</sup>-E TPUD PAEK-HTS45, is a thermoplastic unidirectional (TPUD) prepreg, combining high-strength carbon fiber and LM PAEK. The prepreg tape was slit to prepreg tows with 6.35 mm (1/4 in.) in width and a nominal thickness of 0.14 mm, and was provided by Teijin Carbon America. The remaining manufacturing parameters are as follows: nozzle temperature, bed temperature, layer thickness,

number of layers, and printing speed. Industry best practices developed in Automated Fiber Placement (AFP) of the TPUD LM PAEK-carbon fiber prepreg are used as guidelines for designing manufacturing trials in this study. Table 2 summarizes 18 tensile specimens designed and fabricated in this investigation along with their average thicknesses from six measurements.

**Table 2. Manufacturing trials for tensile specimens per ASTM D3039-17 from TPUD prepreg.**

Specimen #	Nozzle temperature (°C)	Bed temperature (°C)	Layer thickness (mm)	Number of layers	Average thickness (mm)
1-1	420	160	0.2	5	1.08
2-1	420	30	0.2	5	0.75
3-1	420	30	0.2	5	0.71
4-1	420	30	0.2	6	0.95
5-1	420	160	0.2	6	0.91
6-1	380	30	0.2	6	0.90
7-1 to 7-5	380	30	0.15	7	0.90 1.02 0.88  0.98 1.08
8-1 to 8-7	380	165	0.15	7	0.86 0.95 0.91 0.84  0.94 0.95 0.91

Specimens were visually inspected after 3D printing, and sent to an ISO/CEI 17025:2017 accredited testing laboratory, where they were trimmed to a length of 250 mm per ASTM D3039-17 standard. Since tensile specimens are 3D printed individually with a 6.35 mm prepreg tows, the nominal width of the specimens is 19.05 mm (3 prepreg tows side by side). Specimen set #7 is provided in Figure 3, which shows a high surface quality without any visible defect.

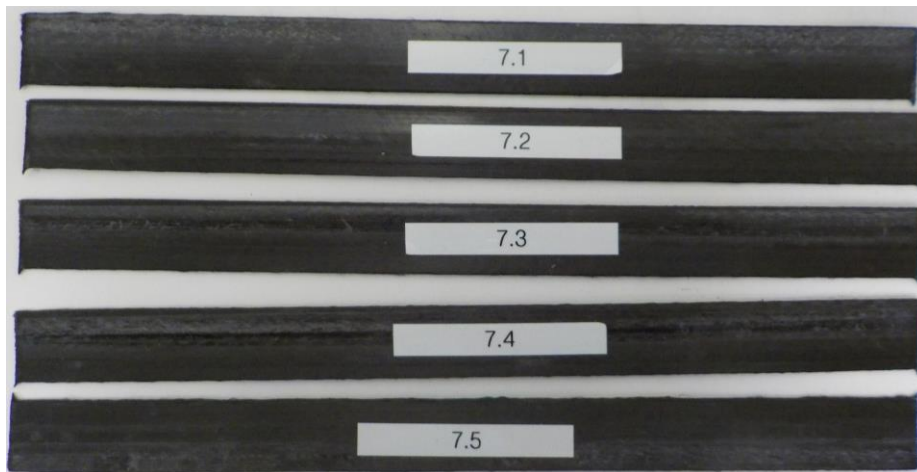


**Figure 3. Specimen set #7 after trimming and before tensile testing.**

A high-precision hydraulic testing machine (Dynamometer Zwick Z250 All-Around) with a load capacity of 250 kN and a biaxial extensometer with a 25% strain limit were used for tensile



testing at a constant head speed of 2 mm/min. Thermal testing by Differential Scanning Calorimetry (DSC) was performed to find the degree of crystallinity for specimen sets #7 and 8 using the trim leftovers from 7-1 and 8-2 tensile specimens. In addition, SEM imaging of the cross-section for specimen 7-1 was completed.

### 3. Results and discussion

Emery cloth was used to grip the specimens without damaging them, which in combination with high precision hydraulic testing machine resulted in acceptable failure mode and location for all specimens. Therefore, per Section 8.2.1.2 of ASTM D3039, emery cloth was proved to be sufficient for tensile testing of the 3D printed specimens, and bonded tabs were not used. Figure 4 shows the stress-strain graph for specimen 7-1, and Figure 5 shows specimen set #7 after failure.

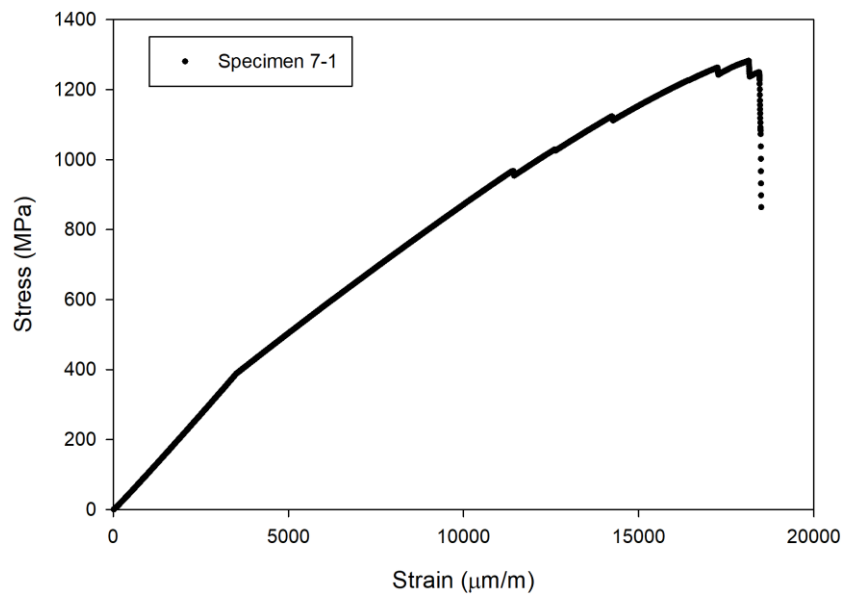


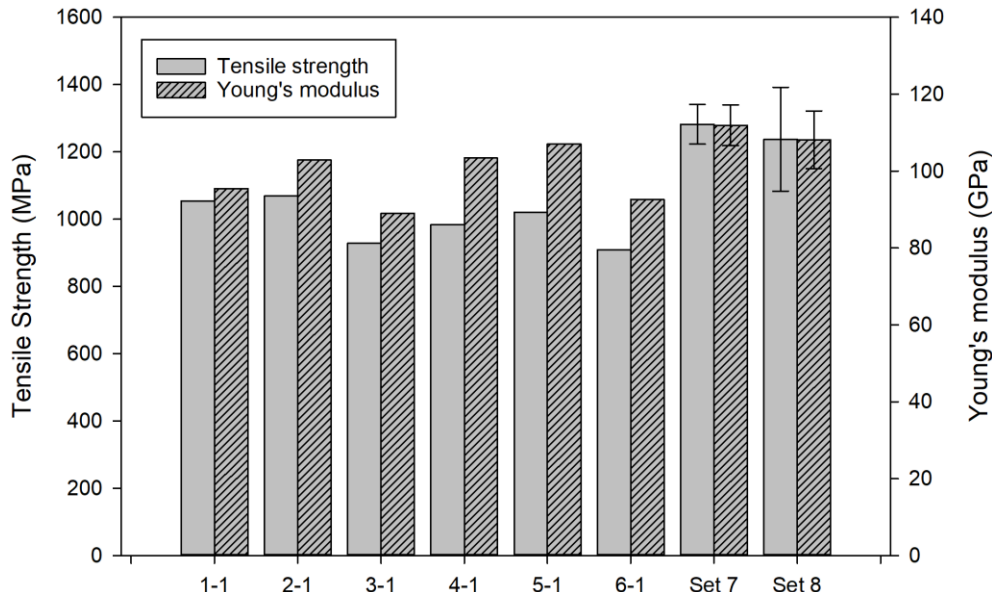
Figure 4. Stress-strain curve for specimen 7-1.



Figure 5. Specimen set 7 after tensile testing.

According to ASTM D3039-17, Young's modulus and Poisson's ratio must be calculated between 1000 and 3000  $\mu\text{m/m}$  strain. Therefore, the strain recording until 4000  $\mu\text{m/m}$  was completed using the bi-axial extensometer for accurate measurements, and was changed to the grip displacement until specimen failure. After 4000  $\mu\text{m/m}$  strain, strain is measured with less precision for the same stress, resulting in a reduced slope in the stress-strain graph (Figure 4). Multiple kinks are observed in the stress-strain curve, which shows the failure of some continuous carbon fibers during the test and the redistribution of load among remaining carbon fibers until complete specimen failure. These kinks were observed for almost all tensile specimens tested in this study. Figure 5 shows failure in all specimens started from the gage section (not the grips), and the failure code is SMV, i.e., long splitting, multiple areas, and various locations. It should be noted that all the other tensile specimens in this study exhibited the same failure mode, SMV.

Figure 6 shows tensile strength and modulus of all 18 specimens (see Table 2) calculated per ASTM D3039.



**Figure 6. Tensile strength and modulus of all the 18 specimens.**

Specimen sets 7 and 8 exhibited the highest tensile strength and Young's modulus; therefore, they are examined in more detail. The maximum normed residual (MNR) method was used to screen tensile strength, Young's modulus, and failure strain results for outliers. It was found that the MNR values for all test results are below the critical value of 1.715 and 2.020 for a sample size of five and seven, respectively [23]. Therefore, all tensile property results for specimen sets 7 and 8 are used in the statistical calculations, mean and Coefficient of Variation (CV) in Table 3. For specimen set 7, the CV is less than 5% for tensile strength and Young's modulus, while it is less than 10% for failure strain. These CV values are well within acceptable ranges for showing the manufacturing and tensile testing robustness. The CV for specimen set 8 is higher than specimen set 7 for all tensile properties, especially failure strain. It should be noted that the CV is still below and close to 10% for Young's modulus and tensile strength, respectively.

**Table 3. Tensile properties of specimen sets 7 and 8.**

Specimen set	Tensile strength		Young's modulus		Failure strain	
	Mean (MPa)	CV (%)	Mean (GPa)	CV (%)	Mean (%)	CV (%)
7	1282.1	4.6	111.9	4.7	1.8	7.7
8	1237.7	12.5	108.1	6.9	1.7	22.2

Welch's t-test is performed to compare tensile strength, Young's modulus, and failure strain of specimens sets 7 and 8. It should be noted that since specimens sets 7 and 8 have a different number of samples and variances, Welch's t-test is more appropriate than a Student's t-test. It was found that there is not a statistically significant difference between tensile strength ( $P = 0.508$ ), Young's modulus ( $P = 0.328$ ), and failure strain ( $P = 0.604$ ) of specimens sets 7 and 8. A summary of tensile properties of 3D printed continuous fiber reinforced composites made from FFF 3D printing is provided in Table 1. The maximum reported values for thermoplastic composites were by Blok et al. [4], who obtained tensile strength and modulus of 968 MPa and 62.5 GPa, respectively, for Nylon-carbon fiber. Specimen set 7 in our study shows 32.4% and 79.0% improvement in tensile strength and modulus, respectively, compared with Blok et al. [4]. In addition, LM PAEK-carbon fiber specimens investigated in our study have a higher operating temperature and wider industrial applications than Nylon-carbon fiber.

To indicate the continuous carbon fiber reinforcement effect, a custom-built gantry-based high-temperature 3D printer was used to fabricate pure LM PAEK specimens per ASTM D638-14 type II from AM<sup>TM</sup> 200 filament. This feedstock is an LM PAEK co-polymer provided by Victrex, which has essentially the same polymer chain as the one in the continuous carbon fiber prepreg used in robotic 3D printing of tensile specimens per ASTM D3039-17 (Table 2). The manufacturing process and design parameters for the pure LM PAEK dog-bone specimens are summarized in Table 4.

**Table 4. Manufacturing and design parameters for dog-bone tensile specimen 3D printing.**

Manufacturing/design parameter	Value	Manufacturing/design parameter	Value
Print direction	XYZ	Material	AM <sup>TM</sup> 200
Filament diameter	1.75 mm	Nozzle diameter	0.6 mm
Layer height	0.25 mm	Nozzle temperature	360 °C
Bed and chamber temperature	160 °C	Cooling	N/A
Printing speed	30 mm/s	Infill percentage	100%

An infill pattern was optimized to provide a 0° raster angle in the gage section of the dog-bone specimens without any voids in the transition areas (Figure 7a). Five specimens were 3D printed, weighed, and their dimensions were measured before tensile testing (Figure 7b). They were removed no more than 5 minutes after the end of the print, with the chamber temperature maintained, and immediately sandwiched between two 1/4 in. thick steel plates. The plate-quench intended to rapidly cool the coupons to room temperature while minimizing the warpage of the final part. While there are some areas of under-extrusion in the grip section, the gage section in all specimens is fabricated without any defects, which is essential for accurate tensile properties measurement.

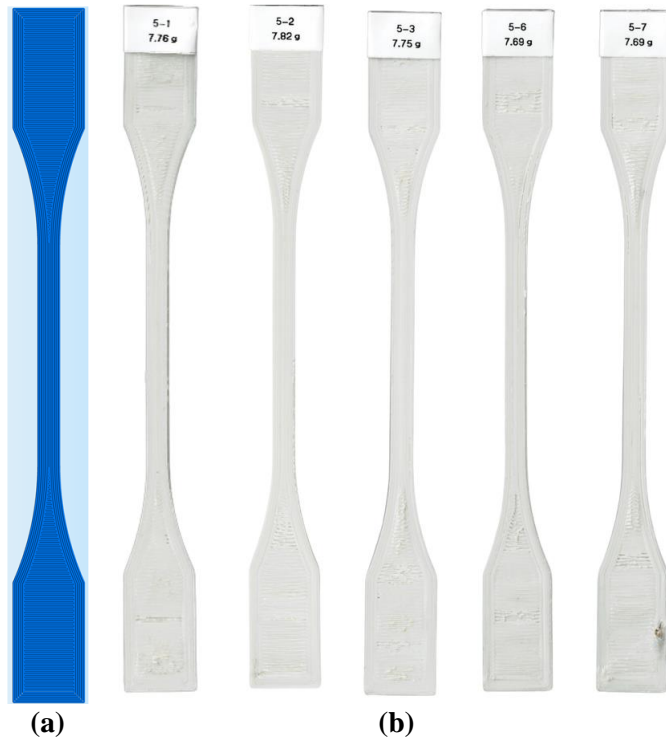


**Figure 7. Dog-bone tensile specimens per ASTM D638-14 type II: (a) optimized infill; and (b) five 3D printed specimens from AM™ 200.**

A uniaxial mechanical testing machine with a 2.22 kN (500 lbf) load cell was used for testing with a constant crosshead displacement rate of 5 mm/min and a 25-mm gage length clip-on extensometer for measuring strain. Mean tensile strength of 78.9 MPa (CV: 3.6%) and tensile modulus of 3.30 GPa (CV: 4.7%) were obtained. It should be noted that specimen set 7 made from LM PAEK reinforced with continuous carbon fiber had a tensile strength and modulus of 1282.1 MPa and 111.9 GPa, respectively. These values for tensile strength and modulus are about 16 and 34 times higher than those obtained for pure LM PAK specimens.

A DSC Q250 (TA Instruments, New Castle, USA) was used for thermal testing to determine the glass transition temperature, enthalpies of fusion, and degree of crystallinity for specimens 7-1 and 8-2 per ASTM D3418-15. Samples of 10.30 mg and 11.00 mg were used from the trim leftovers of specimens 7-1 and 8-2, respectively. A standard aluminum pan with a diameter of 6.4 mm and a mass of 11 mg was utilized. The sample atmosphere was nitrogen with a purity of 99.998% and a 50 ml/min flow rate. Temperature calibration was performed per ASTM E967-18 with a baseline ramp from -90 °C to 400 °C at a rate of 10 °C/min and a ramp for indium from 106.56 °C to 186.56 °C at a rate of 10 °C/min. After the calibration, a heating ramp from 20 °C to 400 °C at 10 °C/min is used with a hold time of 5 min, followed by a cooling ramp to 20 °C with the same rate and hold time. The second heating ramp is applied with the same parameters as the first one. Figure 8a and 8b show the DSC curves for the first heating (green), cooling (red), and second heating ramps (orange) for specimens 7-1 and 8-2, respectively.

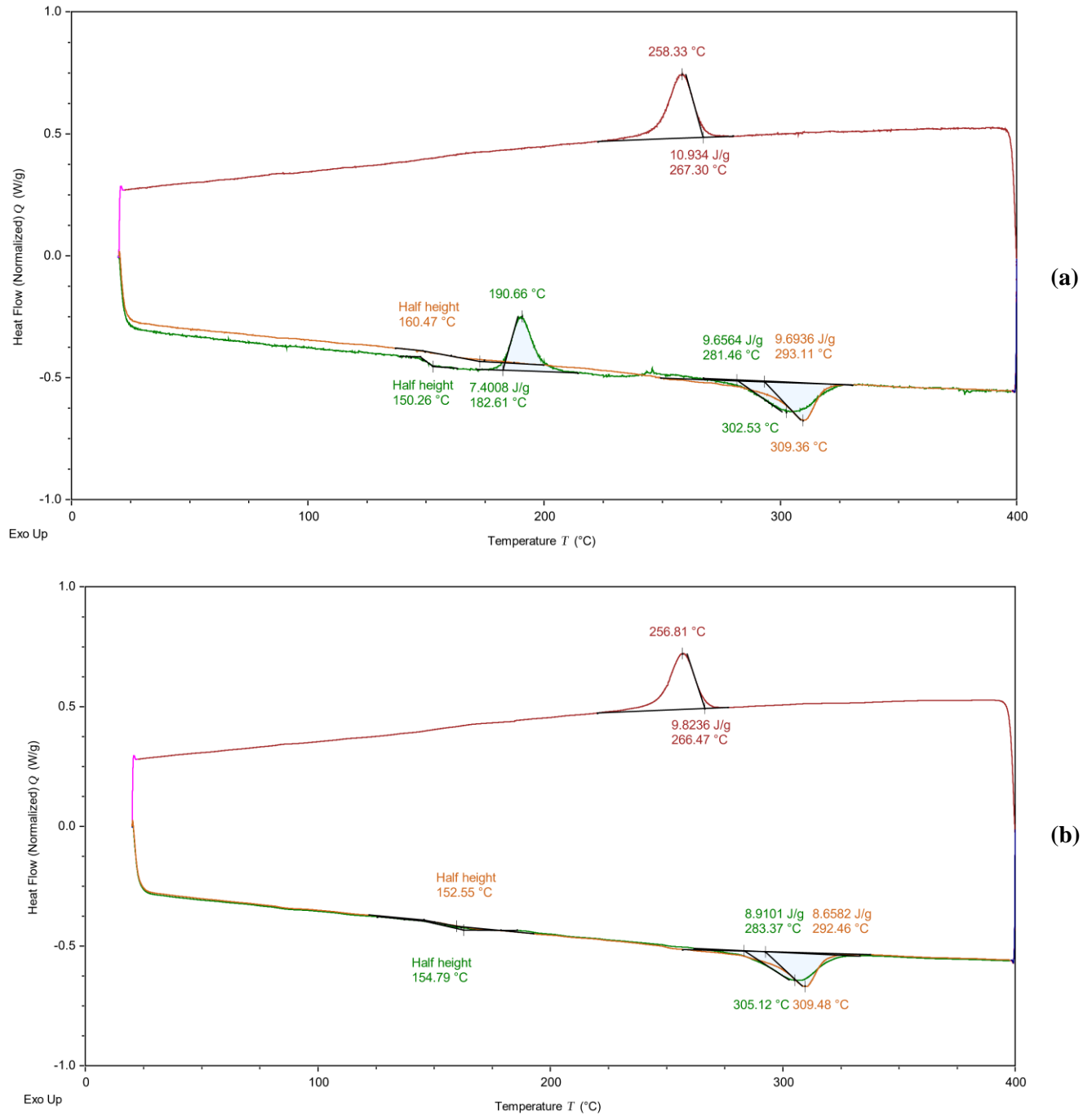


**Figure 8. DSC thermograms for the first heating (green), cooling (red), and second heating ramps (orange) for two specimens (a): specimen 7-1; and (b): specimen 8-2.**

The results from the DSC test for specimens 7-1 and 8-2 are summarized in Table 5. It should be noted that the midpoint temperature ( $T_{mg}$ ) is designated as the glass transition temperature ( $T_g$ ).

**Table 5. The DSC test results for specimens 7-1 and 8-2.**

<b>Parameter</b>	<b>Specimen 7-1</b>	<b>Specimen 8-2</b>
<b>First heating ramp</b>		
Glass transition temperature (°C)	150.26	154.79
Crystallization extrapolated onset temperature (°C)	182.61	N/A
Crystallization peak temperature (°C)	190.66	N/A
Melting extrapolated onset temperature (°C)	281.46	283.37
Melting peak temperature (°C)	302.53	305.12
Enthalpy of fusion (J/g)	9.6564	8.9101
<b>Cooling ramp</b>		
Crystallization extrapolated onset temperature (°C)	267.30	266.47
Crystallization peak temperature (°C)	258.33	256.81
Enthalpy of crystallization (J/g)	10.934	9.8236
<b>Second heating ramp</b>		
Glass transition temperature (°C)	160.47	152.55
Melting extrapolated onset temperature (°C)	293.11	292.46
Melting peak temperature (°C)	309.36	309.48
Enthalpy of fusion (J/g)	9.6936	8.6582

Since the impact of 3D printing process parameters on thermal properties of the specimens as manufactured is of interest,  $T_g$  and degree of crystallinity are calculated from the first heating ramp. The  $T_g$  for specimens 7-1 and 8-2 is 150.26 °C and 154.79 °C, respectively. It should be noted that the heating curve for specimen 8-2 did not show a clear glass transition; therefore, the manual point picking can be the reason behind the difference between the  $T_g$  values. A cold crystallization was observed for specimen 7-1 with an enthalpy of 7.4008 J/g, while specimen 8-2 did not exhibit this and reached an acceptable level of crystallinity after 3D printing. The degree of crystallinity for specimens 7-1 and 8-2 was calculated using the enthalpy of fusion of 100% crystalline LM PAEK of 130 J/g and polymer content in the TPUD prepreg of 34%. The degree of crystallinity was 5.10% and 20.2% for specimens 7-1 and 8-2, respectively. As seen in Table 2, the only difference in the manufacturing parameters between specimen sets 7 and 8 is the build platform temperature. Specimen set 7 was 3D printed on a 30 °C build platform, while specimen set 8 was manufactured on a 165 °C plate. The DSC test shows the importance of a build platform heated above the  $T_g$  to ensure an acceptable level of crystallization (no cold crystallization), thereby removing the need for a post-process annealing and increasing the chemical resistance of the parts.

Scanning Electron Microscope (SEM) images from the cross-section of specimen 7-1 outside the gage after tensile testing were obtained at two magnification levels. Figure 9a shows the cross-section at 50X magnification, while Figure 9b and c illustrate different parts of the cross-section at 200X magnification. Figure 9a confirms that the specimen is consolidated completely, and only minimal gaps can be observed between different plies. In addition, at higher magnification levels, a uniform distribution of fibers and minimum voids within each ply are found. It should be noted that specimen 7-1 has a stacking sequence of  $[0]_7$ . Other layups, e.g.,

quasi-isotropic with fibers at  $0^\circ$ ,  $90^\circ$ , and  $\pm 45^\circ$ , will be used for creating micrographs in future studies.

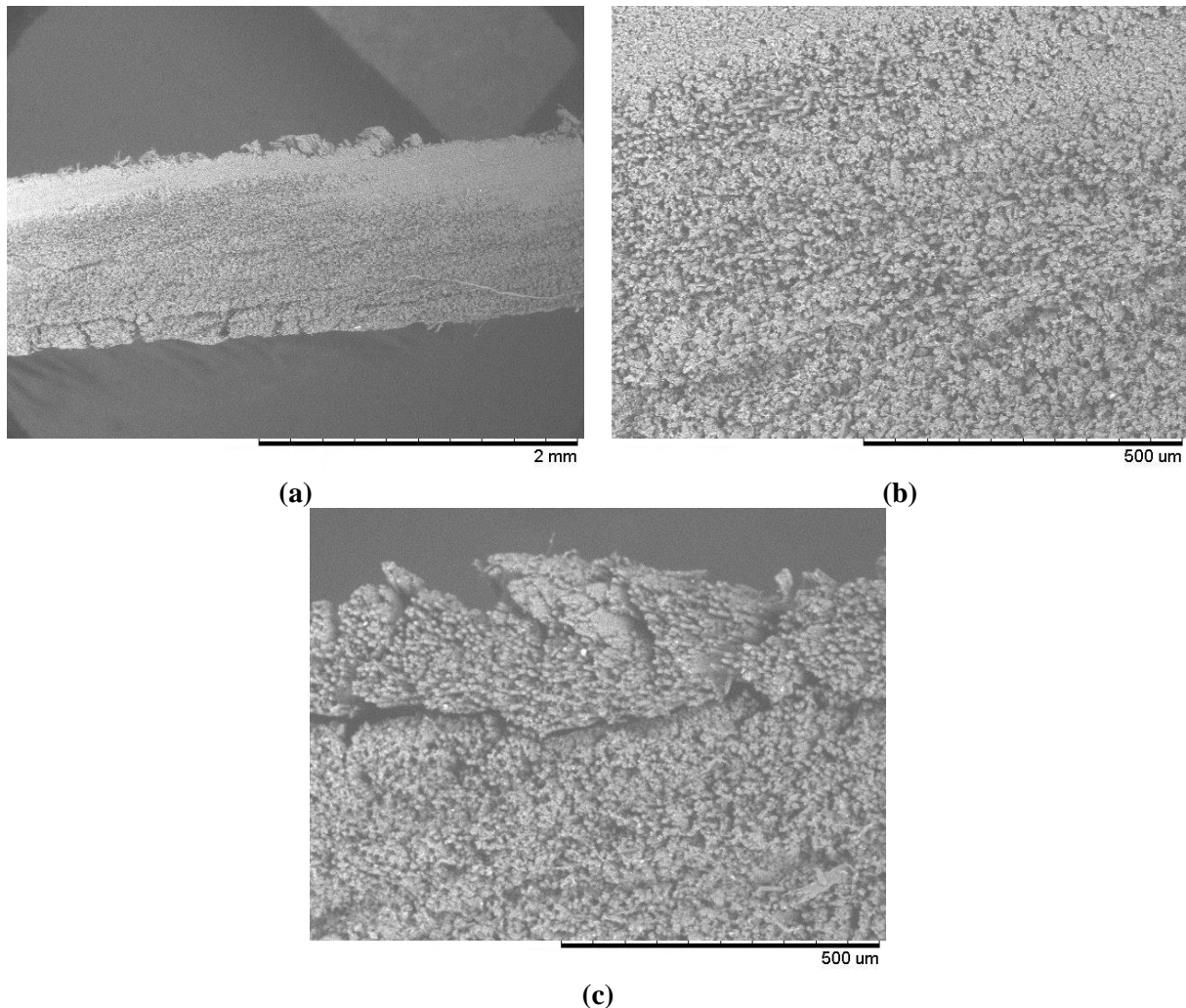


**Figure 9. SEM images of specimen 7-1 at different magnification levels: (a) 50X; (b) 200X; and (c) 200X.**

The tensile and DSC testing results show that optimum 3D printing process parameters for LM PAEK-carbon fiber in this study are nozzle temperature of  $380^\circ\text{C}$ , bed temperature of  $165^\circ\text{C}$ , and layer thickness of  $0.15\text{ mm}$ . The optimum 3D printing process parameters can be used to manufacture specimens per ASTM D5379-19 to evaluate their in-plane and interlaminar shear properties, and will be investigated in a future study. In addition, complex parts like a composite elbow and a rudder will be manufactured to show the robotic 3D printing applications and manufacturing feasibility.

#### **4. Conclusions**

A six-axis ABB IRB1200 robot with a custom-built 3D printing head as an end effector has been utilized for manufacturing parts from Low-Melt Poly Aryl Ether Ketone (LM PAEK) reinforced with continuous carbon fiber. A slotted nozzle hardened to 54-58 RC has been designed

and fabricated with a 304.8 × 304.8 mm (12 × 12 in) stainless-steel heated build platform. Nozzle and bed temperatures were monitored and controlled with a programmable logic controller (PLC) box. The feedstock was Tenax<sup>TM</sup>-E TPUD PAEK-HTS45 slit to prepreg tows with 6.35 mm (1/4 in) in width and a nominal thickness of 0.14 mm. A total of 18 tensile specimens per ASTM D3039-17 with 0° fiber orientation were 3D printed flat on the build platform. Nozzle temperature, bed temperature, layer thickness, and the number of layers were varied. Trim leftovers were used to perform DSC testing per ASTM D3418-15 and SEM imaging.

Failure mode was acceptable for all tensile specimens, and the failure code was SMV, i.e., long splitting, multiple areas, and various locations. The maximum tensile strength, modulus, and failure strain were 1282.1 MPa, 111.9 GPa, and 1.8%, respectively. These tensile strength and modulus show an improvement of 32.4% and 79.0% in tensile strength and modulus, respectively, compared with the maximum reported values in the literature for thermoplastic composites made from FFF 3D printing. DSC testing showed a  $T_g$  of 154.79 °C for an LM PAEK-CF specimen 3D printed with a nozzle and bed temperatures of 380 °C and 165 °C, respectively. The specimen did not show a cold crystallization during the DSC test, and had a degree of crystallinity of 20.2%. However, the specimen manufactured on a 30 °C build plate exhibited a cold crystallization in the first heating curve, and only reached 5.10% degree of crystallinity. SEM images showed a uniform distribution of fibers, minimum voids within each ply, and minimal gaps between layers.

This study investigated the tensile and thermal properties of 3D printed LM PAEK-CF specimens. In addition to tensile testing, in-plane and interlaminar shear properties per ASTM D5379-19 can indicate 3D printed parts' quality and will be explored as future work. Furthermore, a quasi-isotropic layup with 0°, 90°, and ±45° fiber orientations can be used for micrograph analysis.

## Acknowledgment

We want to thank Levi Gregorash and Sadben Khan for the design and manufacturing of the PLC box and the initial version of the 3D printing head. In addition, the help from Kimia Abedi for manufacturing trials is greatly appreciated.

## References

- [1] Van Der Klift, F., Koga, Y., Todoroki, A., Ueda, M., Hirano, Y. and Matsuzaki, R., 2016. 3D printing of continuous carbon fibre reinforced thermo-plastic (CFRTP) tensile test specimens. *Open Journal of Composite Materials*, 6(01), p.18.
- [2] Melenka, G.W., Cheung, B.K., Schofield, J.S., Dawson, M.R. and Carey, J.P., 2016. Evaluation and prediction of the tensile properties of continuous fiber-reinforced 3D printed structures. *Composite Structures*, 153, pp.866-875.
- [3] Oztan, C., Karkkainen, R., Fittipaldi, M., Nygren, G., Roberson, L., Lane, M. and Celik, E., 2019. Microstructure and mechanical properties of three dimensional-printed continuous fiber composites. *Journal of Composite Materials*, 53(2), pp.271-280.



- [4] Blok, L.G., Longana, M.L., Yu, H. and Woods, B.K., 2018. An investigation into 3D printing of fibre reinforced thermoplastic composites. *Additive Manufacturing*, 22, pp.176-186.
- [5] Dickson, A.N., Barry, J.N., McDonnell, K.A. and Dowling, D.P., 2017. Fabrication of continuous carbon, glass and Kevlar fibre reinforced polymer composites using additive manufacturing. *Additive Manufacturing*, 16, pp.146-152.
- [6] Mei, H., Ali, Z., Ali, I. and Cheng, L., 2019. Tailoring strength and modulus by 3D printing different continuous fibers and filled structures into composites. *Advanced Composites and Hybrid Materials*, 2(2), pp.312-319.
- [7] González-Estrada, O.A., Pertuz, A. and Quiroga Mendez, J.E., 2018. Evaluation of tensile properties and damage of continuous fibre reinforced 3D-printed parts. In *Key Engineering Materials* (Vol. 774, pp. 161-166). Trans Tech Publications Ltd.
- [8] Naranjo-Lozada, J., Ahuett-Garza, H., Orta-Castañón, P., Verbeeten, W.M. and Sáiz-González, D., 2019. Tensile properties and failure behavior of chopped and continuous carbon fiber composites produced by additive manufacturing. *Additive Manufacturing*, 26, pp.227-241.
- [9] Pyl, L., Kalteremidou, K.A. and Van Hemelrijck, D., 2018. Exploration of specimen geometry and tab configuration for tensile testing exploiting the potential of 3D printing freeform shape continuous carbon fibre-reinforced nylon matrix composites. *Polymer Testing*, 71, pp.318-328.
- [10] Matsuzaki, R., Ueda, M., Namiki, M., Jeong, T.K., Asahara, H., Horiguchi, K., Nakamura, T., Todoroki, A. and Hirano, Y., 2016. Three-dimensional printing of continuous-fiber composites by in-nozzle impregnation. *Scientific reports*, 6, p.23058.
- [11] Gardner, J.M., Sauti, G., Kim, J.W., Cano, R.J., Wincheski, R.A., Stelter, C.J., Grimsley, B.W., Working, D.C. and Siochi, E.J., 2016. 3-D printing of multifunctional carbon nanotube yarn reinforced components. *Additive Manufacturing*, 12, pp.38-44.
- [12] Yin, L., Tian, X., Shang, Z., Wang, X. and Hou, Z., 2019. Characterizations of continuous carbon fiber-reinforced composites for electromagnetic interference shielding fabricated by 3D printing. *Applied Physics A*, 125(4), p.266.
- [13] Yang, C., Tian, X., Liu, T., Cao, Y. and Li, D., 2017. 3D printing for continuous fiber reinforced thermoplastic composites: mechanism and performance. *Rapid Prototyping Journal*.
- [14] Li, N., Li, Y. and Liu, S., 2016. Rapid prototyping of continuous carbon fiber reinforced polylactic acid composites by 3D printing. *Journal of Materials Processing Technology*, 238, pp.218-225.
- [15] Akhoundi, B., Behraves, A.H. and Bagheri Saed, A., 2019. Improving mechanical properties of continuous fiber-reinforced thermoplastic composites produced by FDM 3D printer. *Journal of Reinforced Plastics and Composites*, 38(3), pp.99-116.
- [16] Chanteli, A., Bandaru, A.K., Peeters, D., O'Higgins, R.M. and Weaver, P.M., 2020. Influence of repress treatment on carbon fibre-reinforced PEEK composites manufactured using laser-assisted automatic tape placement. *Composite Structures*, 248, p.112539.
- [17] Yi, N., Davies, R., Chaplin, A., McCutcheon, P. and Ghita, O., 2021. Slow and fast crystallising poly aryl ether ketones (PAEKs) in 3D printing: Crystallisation kinetics, morphology, and mechanical properties. *Additive Manufacturing*, 39, p.101843.
- [18] Zhang, X., Li, M., Lim, J.H., Weng, Y., Tay, Y.W.D., Pham, H. and Pham, Q.C., 2018. Large-scale 3D printing by a team of mobile robots. *Automation in Construction*, 95, pp.98-106.
- [19] Farahbakhsh, M., Rybkowski, Z.K., Zakira, U., Kalantar, N. and Onifade, I., 2022. Impact of robotic 3D printing process parameters on interlayer bond strength. *Automation in Construction*, 142, p.104478.

[20] Bedarf, P., Szabo, A., Zanini, M., Heusi, A. and Dillenburger, B., 2022. Robotic 3D Printing of Mineral Foam for a Lightweight Composite Concrete Slab. Proceedings of the 27th International Conference of the Association for Computer-Aided Architectural Design Research in Asia (CAADRIA) 2022, Volume 2, 61-70.

[21] Hannah Mason and Ginger Gardiner (2020) 3D printing with continuous fiber: A landscape. <https://www.compositesworld.com/articles/3d-printing-with-continuous-fiber-a-landscape>. Accessed 4 August 2022.

[22] ISO/ASTM 52921, Standard Terminology for Additive Manufacturing—Coordinate Systems and Test Methodologies, (2013), pp. 1–13.

[23] MIL-HDBK-17F (2002) The Composite Materials Handbook. Volume 1: Polymer Matrix Composites Guidelines for Characterization of Structural Materials, ASTM International, West Conshohocken PA.

## **Statements & Declarations**

### **Funding**

Financial support from the Natural Sciences and Engineering Research Council of Canada (NSERC), RGPIN-2018-04144, and Mitacs accelerate programs, IT22530, helped this investigation.

### **Data availability statement**

The raw/processed data required to reproduce these findings cannot be shared at this time as the data also forms part of an ongoing study.

### **Competing Interests**

The authors have no relevant financial or non-financial interests to disclose.

### **Author Contributions**

Seyed Miri, Jordan Kalman, and Kazem Fayazbakhsh contributed to the study conception and design. Seyed Miri and Jordan Kalman performed material preparation, data collection, and analysis. Kazem Fayazbakhsh wrote the first draft of the manuscript, and all authors reviewed and provided comments regarding previous versions of the manuscript. Jean-Philippe Canart and Joe Spangler contributed to the conceptualization of the study and provided resources. Kazem Fayazbakhsh administered the project and supervised the students. All authors read and approved the final version of the manuscript.